最近の研究から

Si(111)-$\sqrt{3}$ ×$\sqrt{3}$ -Ag 表面上における原子レベルでの金ナノクラスターの自己組織化

劉　燦華，松田　巌，長谷川　修司
東京大学大学院理学系研究科物理学専攻

Atomic self-assembly of Au nanoclusters on the Si(111)-$\sqrt{3}$ × $\sqrt{3}$-Ag surface

Canhua Liu, Iwao Matsuda, and Shuji Hasegawa
Department of Physics, School of Science, University of Tokyo

1. Introduction

The fabrication methods of the microelectronics industry have been refined to produce even smaller devices, but will soon reach their fundamental limits. A promising alternative route to even smaller functional system with nanometer dimensions is the autonomous ordering and assembly of atoms and molecules on atomically well-defined surfaces. It has been turned out, for example, that a Si(111)-7 × 7 surface is an ideal template due to its dangling bonds which may assign periodic adsorption sites to foreign atoms [1]. The role of interactions among nanoclusters themselves is negligible in this kind of self-assembly process. On a smooth surface where adsorbates bond to the substrate weakly, in contrast, the interactions among adatoms should have more important influence on the formation of nanostructure arrays. On some metal surfaces, for example, surface state mediated adatom interactions are believed to play significant roles in the atomic self-assembly [2]. In previous studies, scanning tunneling microscopy (STM) has been well employed to reveal the processes and mechanisms of the self-assembly due to its powerful atomic resolutions in topography. However, photoemission spectroscopy (PES) has been few reported in spite that it provides precise information on electronic structures that might be modified in the self-assembly process.

A monolayer-Ag-terminated Si(111) surface, the Si(111)-$\sqrt{3}$×$\sqrt{3}$-Ag surface ($\sqrt{3}$-Ag in short hereafter), is an ideal substrate for studying this issue because of its intactness against adsorbates owing to no dangling bonds remaining on the surface [3, 4]. In addition, it has a surface state of two-dimensional nearly-free electron gas (2DEG) which can mediate the indirect electronic adatom-adatom interactions [5]. In this report, we first introduce our recent STM observations of 2D identical Au nanoclusters on the $\sqrt{3}$-Ag surface, and their self-assembly into the Si(111)-$\sqrt{21}$×$\sqrt{21}$ -(Ag+Au) superstructure ($\sqrt{21}$ -Au in short hereafter). With Si 2*p* core level spectra (CLS) of the $\sqrt{3}$-Ag and $\sqrt{21}$-Au surfaces, we determined that each Au nanocluster consists of three Au adatoms, which helped to propose a new atomic structure model of the $\sqrt{21}$-Au surface [6]. Using angle-resolved PES, in the end, we investigated changes in the 2DEG band of the Au nanoclusters dispersed $\sqrt{3}$-Ag, revealing that the band split into two due to its hybridization with adatom-induced localized states. [5].

2. Self-assembly of 2D Au nanoclusters

Submonolayer Au adsorption on the $\sqrt{3}$-Ag surface has been well studied previously as well as other noble and alkali metals [3, 7-17]. An interesting point is that the adsorptions of these monovalent atoms commonly induce $\sqrt{21}$×$\sqrt{21}$ surface superstructures, which have elevated surface electrical conductivities comparing to the $\sqrt{3}$-Ag substrate due to electron transfer [12-17]. In spite of extensive experimental and theoretical studies [7-12], the atomic structure of$\sqrt{21}$ × $\sqrt{21}$ surfaces are still under debate and their formation mechanism is unclear.

All of the previous STM studies on the $\sqrt{21}$-Au superstructures had been performed only at room temperature (RT) [8, 9], in which a remarkable feature is that the $\sqrt{21}$-Au domain boundary changes successively and appears vague due to incessant attachment and detachment of Au atoms at the domain periphery [6]. To reduce the migration of Au adatoms, we cooled the Au-adsorbed $\sqrt{3}$-Ag surface to 65 K for STM observations.

Fig. 1 shows a series of topographic STM images taken at 65 K from Au adsorbed $\sqrt{3}$-Ag surface. At the very beginning of Au adsorption (0.016 ML), isolated Au nanoclusters distribute randomly on the surface and exhibit identical shape, as shown in Fig. 1(a). When the Au coverage is increased up to 0.048

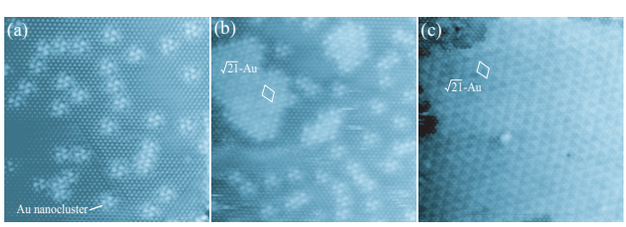

Figure 1 Topographic STM images of Au-adsorbed $\sqrt{3}$-Ag surface taken at 65 K and at various Au coverages: (a) 0.016 ML, V_{tip} = −0.50 V, I = 0.75 nA; (b) 0.048 ML, V_{tip} = −0.50 V, I = 0.75 nA; (c) 0.136 ML, V_{tip} = −1.50 V, I = 0.50 nA. The size of each image is 31.2 × 31.2 nm^2.

ML in Fig. 1(b), small domains of the $\sqrt{21}$-Au superstructure are formed. At Au coverage of 0.136 ML in Fig. 1(c), the $\sqrt{21}$-Au domains grow largely in size and cover almost the whole surface.

Fig 2(a) is an enlarged STM image containing a small $\sqrt{21}$-Au domain together with isolated identical Au nanoclusters. Giving a sign of an Au nanocluster with a circle, we found that the $\sqrt{21}$-Au domain can be divided into Au nanoclusters with the same circles. In other words, *the superstructure of* $\sqrt{21}$*-Au can be viewed as a periodic arrangement of the identical Au nanoclusters*. Actually, the whole $\sqrt{21}$-Au domain in Fig 2(a) can be exactly covered by such circles.

The series of STM images at various Au coverages in Fig. 1 thus demonstrate clearly the process of self-assembly of the Au nanoclusters into the $\sqrt{21}$-Au superstructure. At low coverage, the identical Au nanoclusters distribute separately on the surface due to a kind of adatom-adatom interaction via the substrate. When the Au coverage is increased, the Au clusters have to aggregate into the $\sqrt{21}$-Au superstructure because there may be no enough space for them to disperse. This is exactly the formation mechanism of the $\sqrt{21}$-Au surface [6].

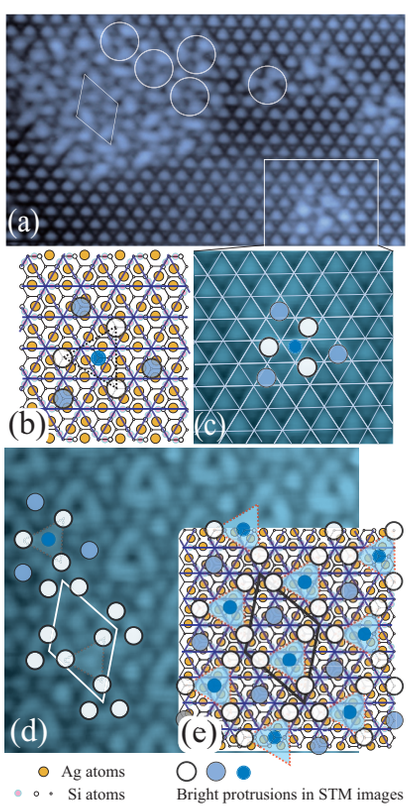

Figure 2 (a) STM image of Au-adsorbed $\sqrt{3}$-Ag surface showing a small $\sqrt{21}$-Au domain and some isolated Au nanoclusters. V_{tip} = −0.30 V, I = 0.75 nA; (b) IET model for the $\sqrt{3}$-Ag, on which several spheres show the relative position of BPs in (c), the STM image of a Au nanocluster; (d) STM image of the $\sqrt{21}$-Au superstructure at V_{tip} = −1.00 V and I = 0.60 nA. One of the Au nanoclusters is indicated with a set of spheres used in (b) and (c). (e) Diagram of BPs in the $\sqrt{21}$-Au surface, whose new atomic structure model can be obtained by putting Au adatoms in the position of the bright spheres.

3. Atomic structures of the Au nanocluster and $\sqrt{21}$-Au superstructure

A full understanding of the self-assembly phenomena requires a proper atomic structure model of the nanocluster arrays for, for example, further theoretical studies. As mentioned above, however, in spite of extensive studies, the atomic structure of the $\sqrt{21}$-Au superstructure is still under debate [7].

In contrast to the previous STM studies that have only analyzed the $\sqrt{21}$-Au superstructure itself [8, 9], we started with the Au nanocluster, the basic building block of the $\sqrt{21}$-Au, because of its relative simplicity. There are seven bright protrusions (BPs) in each Au nanocluster as Fig. 2(a) shows. In Fig. 2(c), a hexagonal lattice net is superimposed on the STM image of an isolated Au nanocluster by following the $\sqrt{3}$-Ag unit cells, whose atomic structure model is schematically shown in Fig. 2(b). The seven BPs are indicated with seven spheres, from which we see that all of them locate in the Ag triangles of the $\sqrt{3}$-Ag. Since the Au nanoclusters are build blocks of the $\sqrt{21}$-Au superstructures, we can easily find the correspondence of the seven BPs in the $\sqrt{21}$-Au STM image, as Figs. 2(d) and 2(e) show. After self-assembly, the three BPs at the corners indicated by light-blue spheres overlap with those of the neighbor nanoclusters, so that there are only five BPs in the $\sqrt{21}$-Au unit cell, as Fig. 2(e) shows. Since it is believed that some or all of the BPs correspond to the Au adatoms [8-12], the atomic structure model will be obtained if we can definitely determine the number of Au adatoms in the $\sqrt{21}$-Au unit cell.

To resolve this problem, we investigated the Si 2*p* CLS of the $\sqrt{21}$-Au superstructure as well as the pristine $\sqrt{3}$-Ag surface, finding that there are three Au atoms in each $\sqrt{21}$-Au unit cell after a careful quantitative analysis [6].

The Si 2*p* CLS of the $\sqrt{3}$-Ag surface have been investigated by many researchers [18, 19]. The most reasonable decomposition of the spectra is shown in Fig. 3(a)~(b), where there are two surface (C_1 and C_2), one bulk (B) and one defect (D) components [6, 18]. The two surface components, C_1 and C_2, which shift from the bulk by 0.32 and 0.12 eV toward higher binding energy, are assigned to the atoms of the first and second Si layer, respectively. The atoms in the third Si layer are in a bulk-like environment and may not give rise to any significant energy shift in the spectra.

When the $\sqrt{21}$-Au superstructure is formed, the Si 2*p* spectra significantly change in shape, as shown in Figs. 3(c)~(d). In the decomposition, it requires three surface components, R_1, R_2 and R_3, which shift from the bulk component by 0.30, 0.14 and 0.44 eV, respectively, toward higher binding energy. By comparing to the energy shift of C_1 and C_2 in the $\sqrt{3}$-Ag surface and their intensity changes between normal and 30° emissions, we assigned both R_1 and R_3 to the first layer Si atoms

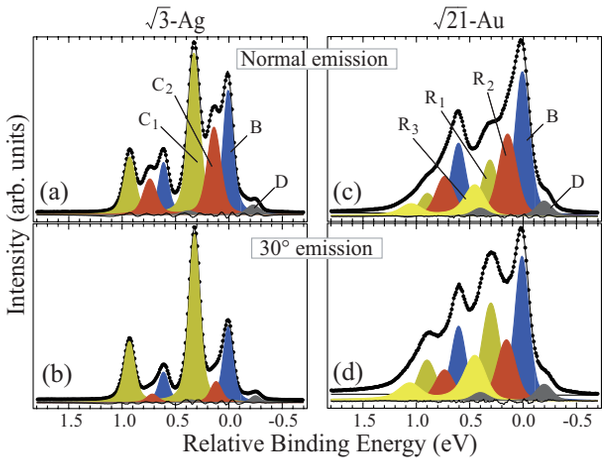

Figure 3 Si 2*p* CLS taken from the $\sqrt{3}$-Ag [(a), (b)] and $\sqrt{21}$-Au [(c), (d)], recorded at 70 K with photon energy of 135 eV at normal [(a), (c)] and 30° [(b), (d)] emissions. The spectra were taken on the beam line of BL-1C at the Photon Factory.

while R_2 to the second layer. The first layer Si atoms are thus divided into two groups. One contributes to R_1 that has an almost identical energy shift as that of C_1. These first layer Si atoms are affected very weakly by Au adatoms. The other first layer Si atoms contribute to R_3, whose larger energy shift indicates a considerable modification of chemical surrounding induced by Au adatoms.

The $\sqrt{3}$-Ag substrate is formed by 1 ML Ag adsorption on the Si(111) crystal surface, which means each Ag atoms saturates one Si dangling bond. Since Au adatoms locate on Ag triangles, each Au adatom may considerably modify the chemical environment of three Si atoms underneath through the Ag triangle. Thus, if the number of Au adatoms in each $\sqrt{21}$-Au unit cell is n, the intensity ratio between R_3 and R_1 should be $3n$: (21 - $3n$). From Figs. 3(c)~(d), we counted that the intensity ratio is 9.4 : 11.6 and 8.2 : 12.8, respectively. Another spectrum taken at 60° emission gives also the ratio of 9.4 : 11.6. All the counted intensity ratios approximate 9 : 12, which implies n = 3, meaning that there are three Au adatoms per $\sqrt{21}$-Au unit cell.

This is a decisive result for determination of the $\sqrt{21}$-Au atomic structure. We see in Fig. 2(d) that the three Au adatoms can only sit at the Ag triangle centers indicated by white spheres due to the three-fold symmetry of the STM images, as long as the BPs correspond to the Au adatoms as believed in previous STM studies.

4. Interaction between adatom induced states and the 2DEG band

As mentioned above, in the self-assembly of Au nanoclusters, adatom-adatom interactions may play significant roles besides the Au-substrate bonds. At a large distance, the Au nanoclusters interact with one anther by conjunctly scattering the 2DEG of the $\sqrt{3}$-Ag substrate. The Au adatoms are centers of attractive potentials to the 2DEG, inducing electronic states localized around [20]. Such bound states hybridize with the 2DEG band and thus modify the spectroscopic signature of the band, which can be revealed by ARPES.

Fig. 4 shows the first ARPES results for this issue [5]. Au adatoms transfer electrons to the $\sqrt{3}$-Ag substrate,shifting the 2DEG band to higher binding energy, as shown in Figs. 4(a)~(b), which were taken at RT from the $\sqrt{3}$-Ag surface with 0.01 and 0.02 ML Au adsorbates thereon, respectively. The 2DEG band deviates from a parabola due to its increased interaction with other two surface bands below as it shifts downwards. A first-principles calculation and STS measurements show that the 2DEG band derives mainly from the Ag p_x and p_y orbitals while the other two surface states consist mainly of Ag 5s orbital with some Ag 5*p* contributions [21]. Using the *s*-like and degenerate *p*-like orbital wave functions, $u_s(\mathbf{r})$ and $u_j(\mathbf{r})$ ($j = x, y$), as the unperturbed basis set, we obtained the dispersion formula, as drawn with solid curves in Figs. 4(a)~(b), for the 2DEG band by a degenerate $\mathbf{k}\cdot\mathbf{p}$ perturbation theory calculation with the Kane model [22]:

$$E(\mathbf{k}_{\parallel}) = E_s - \frac{E_g}{2} + \frac{\hbar^2 k_{\parallel}^2}{2m_0} + \left[\left(\frac{E_g}{2}\right)^2 + \frac{E_g \hbar^2 k_{\parallel}^2}{2m^*}\right]^{\frac{1}{2}} \quad (1)$$

where $E_g = E_s - E_p$, with E_s and E_p the unperturbed energies of the *s* and *p* orbitals at $\mathbf{k} = 0$, respectively. m_0 is the free electron mass and $m^* = \hbar^2 E_g / 2|P|^2$, with $P = -(i\hbar/m_0)\langle u_s | \hat{\mathbf{p}}_j | u_j \rangle$.

Being cooled to 135 K, the 2DEG band was revealed to split into two, as Figs. 4(c)~(d) show. This is exactly the evidence for the interaction between Au adatom induced bound states and the 2DEG band. A general hybridization effect is schematically illustrated in the inset between Figs. 4(c) and

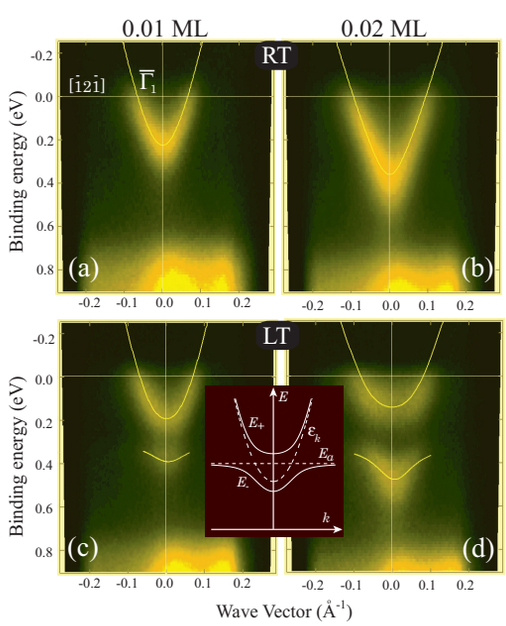

Figure 4 2DEG band of Au adsorbed $\sqrt{3}$-Ag surface taken at (a)~(b) RT and (c)~(d) 135 K. The Au coverages are (a), (c) 0.01 ML and (b), (d) 0.02 ML. Solid lines are fitted results by Eq. (1) [(a)~(b)] and Eq. (3) [(c)~(d)]. The inset between (c) and (d) is a schematic illustration of the hybridization of a conduction band with a localized virtual bound state.

4(d). The conduction band ε_k and the localized virtual bound state E_a before hybridization are shown with dashed lines. After hybridization, the primary band ε_k is split by E_a into two bands, E_+ and E_-.

Because the Au adatoms migrate freely on the surface at RT, it is believed that the adsorption site of each adatom is different. Accordingly, the adatom-induced states may have different energy levels and wave function symmetry, which prevents the formation of an impurity-like band and the hybridization with the 2DEG band. This is the reason that no band splitting is observed in Figs. 4(a)~(b). At 135 K, however, because the Au adatoms are located on equivalent sites on the $\sqrt{3}$-Ag surface, the Au adatom configuration is a subset of the $\sqrt{3}$-Ag crystalline configuration. Therefore, it is possible to include the Au adatom-induced resonant states in the same momentum set as that of the 2DEG band, which is the prerequisite for their hybridization.

Assuming the energy level of the resonant state to be E_a, the Hamiltonian for this 2D system would be

$$H = \sum_{\mathbf{k}\sigma} \left[\varepsilon_{\mathbf{k}} c^{\dagger}_{\mathbf{k}\sigma} c_{\mathbf{k}\sigma} + E_a a^{\dagger}_{\mathbf{k}\sigma} a_{\mathbf{k}\sigma} + V \left(a^{\dagger}_{\mathbf{k}\sigma} c_{\mathbf{k}\sigma} + c^{\dagger}_{\mathbf{k}\sigma} a_{\mathbf{k}\sigma} \right) \right]. \quad (2)$$

The first term describes the unperturbed 2DEG band $\varepsilon_{\mathbf{k}}$ with wave vector $\mathbf{k}$ and spin σ The second term represents the electrons in the adatom-induced band at E_a. The third term accounts for the hybridization between these two bands, with energy V , set to be independent of $\mathbf{k}$ for simplicity. By diagonalizing this Hamiltonian, the hybridized energy dispersion is obtained to be

$$E_{\pm} = \frac{1}{2}\left(\varepsilon_{\mathbf{k}} + E_a\right) \pm \frac{1}{2}\sqrt{\left(\varepsilon_{\mathbf{k}} - E_a\right)^2 + 4V^2}. \quad (3)$$

The unperturbed 2DEG band $\varepsilon_{\mathbf{k}}$ can be obtained from Figs. 4(a)~(b) at RT where the hybridization effect is not yet seen, i.e., $\varepsilon_{\mathbf{k}} = E(\mathbf{k}_{\|})$. Substituting Eq. (1) into Eq. (3), we thus succeeded in reproducing the band dispersion nicely, as the solid curves show in Fig. 4(c)~(d).

After hybridization, it is seen from the split bands in Fig. 4(c)~(d) that there is an energy gap (~ 110 meV)[5], which is described by the hybridization energy V in Eq. (3). An intuitive interpretation of the gap opening is that delocalized electrons in the unperturbed 2DEG band at the energy level E_a are trapped in virtual bound states around the adatoms. It is interesting to note that the 2DEG band of the self-assembled Au nanoclusters, the -$\sqrt{21}$Au surface, has also a gap opening (~ 55 meV) [15], which is exactly half of the hybridization energy. Moreover, both of the gap openings occur at a similar energy level [5, 15]. These results indicate that there is a strong relation between the resonant state and the 2DEG band of the $\sqrt{21}$-Au surface. In other words, the band splitting observed in the ARPES experiment is a strong evidence for that the 2DEG of the $\sqrt{3}$-Ag substrate plays important roles in the self-assembly of the Au nanoclusters, as expected, though further studies are necessary to determine the transition from the impurity state to the continuum state.

5. Conclusion

A self-assembly of 2D nanoclusters on a smooth substrate was demonstrated with submonolayer-Au-adsorbed $\sqrt{3}$-Ag surface. At very low coverage, identical Au nanoclusters are dispersed separately and randomly on the $\sqrt{3}$-Ag surface. As their density is increased, the Au nanoclusters aggregate into the $\sqrt{21}$-Au superstructure. By measuring the Si 2*p* CLS of the self-assembled $\sqrt{21}$-Au surface, we found each Au nanocluster consists of three Au adatoms and thus proposed a new atomic structure model based on the STM observations. Furthermore, ARPES studies revealed that the 2DEG band of the Au nanoclusters dispersed $\sqrt{3}$-Ag surface split into two due to its hybridization with the Au adatom induced bound states. Such an interaction between bound states around the Au adatoms and extensive 2DEG band of the substrate are thought to play important roles in the self-assembly of the Au nanoclusters.

Acknowledgments

Dr. J. Okabayashi and Mr. S. Toyoda are gratefully acknowleged for their help during the CL-PES experiments. This work has been supported by the Grants-In-Aid from the Japanese Society for the Promotion of Science.

References

[1] L. Vitali, M. G. Ramsey and F. P. Netzer, Phys. Rev. Lett. **83**, 316 (1999).

[2] F. Silly, et al., Phys. Rev. Lett. **92**, 016101 (2004).

[3] S. Hasegawa, X. Tong, S. Takeda, N. Sato and T. Nagao, Prog. Surf. Sci. **60**, 89 (1999).

[4] C. Liu, S. Yamazaki, R. Hobara, I. Matsuda, S. Hasegawa, Phys. Rev. B **71**, 041310(R) (2005).

[5] C. Liu, I. Matsuda, R. Hobara and S. Hasegawa, Phys. Rev. Lett. **96**, 036803 (2006).

[6] C. Liu, it el., Phys. Rev. B. **74**, 235420 (2006).

[7] H. Tajiri, K. Sumitani, W. Yashiro, S. Nakatani, T. Takahashi, K. Akimoto, H. Sugiyama, X. Zhang, H. Kawata, Surf. Sci. **493**, 214 (2001).

[8] A. Ichimiya, H. Nomura, Y. Horio, T. Sato, T. Sueyoshi and M. Iwatsuki, Surf. Rev. Lett. **1**, 1 (1994).

[9] J. Nogami, K. J. Wan and X. F. Lin, Surf. Sci. **306**, 81 (1994).

[10] X. Tong, Y. Sugiura, T. Nagao, T. Takami, S. Takeda, S. Ino and S. Hasegawa, Surf. Sci., **408**, 146 (1998).

[11] C. Liu, I. Matsuda and S. Hasegawa, Surf. Interface Anal., **37**, 101 (2005).

[12] X. Tong, S. Ohuchi, N. Sato, T. Tanikawa, T. Nagao, I.

Matsuda, Y. Aoyagi and S. Hasegawa, Phys. Rev. B **64**, 205316 (2001).
[13] X. Tong, C. S. Jiang and S. Hasegawa, Phys. Rev. B **57**, 9015 (1998).
[14] H. M. Zhang, K. Sakamoto and R. I. G. Uhrberg, Phys. Rev. B **64**, 245421 (2001).
[15] J. N. Crain, K. N. Altmann, C. Bromberger and F. J. Himpsel, Phys. Rev. B. **66**, 205302 (2002).
[16] H. M. Zhang, K. Sakamoto and R. I. G. Uhrberg, Phys. Rev. B **70**, 245301 (2004).
[17] I. Matsuda, T. Hirahara, M. Konishi, C. Liu, H. Morikawa, M. D'angelo, S. Hasegawa, T. Okuda and T. Kinoshita, Phys. Rev. B, **71**, 235315, (2005); M. Konishi, I. Matsuda, C. Liu, H. Morikawa and S. Hasegawa, e-J. Surf. Sci. Nanotech. **3**, 107 (2005).
[18] R. I. G. Uhrberg, H. M. Zhang, T. Balasubramanian, E. Landemark and H. W. Yeom, Phys. Rev. B **65**, 081305(R) (2002).
[19] X. Tong, et al., Appl. Surf. Sci. 190, 121 (2002); S. Kono, *et al*., Phys. Rev. Lett. **58**, 1555 (1987); G. S. Herman, *et al*., Surf. Sci. **290**, L643 (1993); G. Le Lay, *et al*., Europhys. Lett. **45**, 65 (1998).
[20] B. Simon, Ann. Phys. (N.Y.) **97**, 279 (1976).
[21] L. Chen, H. J. Xiang, B. Li, A. Zhao, X. Xiao, J. yang, J. G. Hou and Q. Zhu, Phys. Rev. B **70**, 245431 (2004).
[22] J. H. Davies, *The physics of low-dimensional semiconductors,* Cambridge University Press, 1998.

（原稿受付日：2007 年 10 月 9 日）

著者紹介

劉 燦華 Canhua Liu

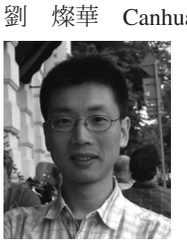

物質･材料研究機構 若手国際研究拠点研究員
〒 305-0044 茨城県つくば市並木 1-1
物質・材料研究機構 若手国際研究拠点
Tel: 029-851-3354ext.8689
Fax: 029-860-4793
e-mail: LIU.Canhua@nims.go.jp

略歴：2006 年東京大学大学院理学系研究科物理学専攻博士課程修了。その後物質・材料研究機構ポスドク研究員。2007 年同若手国際研究拠点研究員。
最近の研究：半導体表面上金属原子ワイヤー配列のプラズモンの研究。固体表面上磁性金属ナノ構造の作成。
趣味：バトミントン。

松田 巌 Iwao Matsuda

東京大学物性研究所 准教授
〒 305-0801 茨城県つくば市大穂 1-1
高エネルギー加速器研究機構
物質構造科学研究所内
Tel: 029-864-1171ext.3890
Tel: 029-864-2489
Fax: 029-864-2461
e-mail: imatsuda@issp.u-tokyo.ac.jp

略歴：2001 年東京大学大学院理学系研究科化学専攻博士課程卒業。理学博士（東京大学）。2000 ～ 2001 年スイス国チューリッヒ大学物理学科にて研究、その後東京大学大学院理学系研究科物理学専攻助手。2006 年より東京大学物性研究所軌道放射物性研究施設准教授，現在に至る。最近の研究：固体表面上金属ナノ構造体の（スピン分解）光電子分光フェルミ面マッピングと磁気伝導の研究。高速時間分解軟Ｘ線分光実験の開発。
最近の趣味：オリーブ栽培 （今年は収穫です）。

長谷川修司 Shuji Hasegawa

東京大学大学院理学系研究科 准教授
〒 113-0033 東京都文京区本郷 7-3-1
東京大学大学院理学系研究科物理学専攻
Tel/Fax. 03-5841-4167
e-mail: shuji@surface.phys.s.u-tokyo.ac.jp

略歴：1985 年 東京大学大学院理学系研究科物理学専攻修士課程修了。理学博士（東京大学 1991 年）。1985 ～ 1990 年 ㈱日立製作所基礎研究所にて研究，その後東京大学大学院理学系研究科物理学専攻助手。1994 年より現職。
最近の研究：表面・ナノ物理。顕微鏡，電子回折，光電子分光，電気伝導など。
最近の趣味：庭の雑草との闘い。